Lumped Parameter Model for Computing the Minimum Pressure During Mechanical Heart Valve Closure

Brant H. Maines
CarboMedics, A Sorin Group Company, Austin,
Texas 78752

Christopher E. Brennen
California Institute of Technology, Pasadena,
California 91125

The cavitation inception threshold of mechanical heart valves has been shown to be highly variable. This is in part due to the random distribution of the initial and final conditions that characterize leaflet closure. While numerous hypotheses exist explaining the mechanisms of inception, no consistent scaling laws have been developed to describe this phenomenon due to the complex nature of these dynamic conditions. Thus in order to isolate and assess the impact of these varied conditions and mechanisms on inception, a system of ordinary differential equations is developed to describe each system component and solved numerically to predict the minimum pressure generated during valve closure. In addition, an experiment was conducted in a mock circulatory loop using an optically transparent size 29 bileaflet valve over a range of conditions to calibrate and validate this model under physiological conditions. High-speed video and high-response pressure measurements were obtained simultaneously to characterize the relationship between the valve motion, fluid motion, and negative pressure transients during closure. The simulation model was calibrated using data from a single closure cycle and then compared to other experimental flow conditions and to results found in the literature. The simulation showed good agreement with the closing dynamics and with the minimum pressure trends in the current experiment. Additionally, the simulation suggests that the variability observed experimentally (when using dP/dt alone as the primary measure of cavitation inception) is predictable. Overall, results from the current form of this lumped parameter model indicate that it is a good engineering assessment tool. [DOI: 10.1115/1.1934164]

Background

The level of interest in heart valve cavitation has risen significantly since reports describing leaflet fracture in 2 Edwards–Duromedics bileaflet valves were released in the late 1980s [1]. The likely location of fracture initiation was reported to occur in regions of pitting. While no definitive conclusion was offered as to the cause of pitting, cavitation erosion is a likely mechanism. As a result, U.S. Food and Drug Administration (FDA) guidelines developed in 1994, require an assessment of the cavitation potential of all new mechanical valves brought to market. Thus it is important to have a full understanding of the mechanism of cavitation inception in order to fulfill FDA requirements, and, more importantly, so that any future mechanical heart valve designs eliminate or minimize the occurrence of cavitation.

Early studies formulated a preliminary list of parameters related to heart valve cavitation inception [2–4]. This list included the physiological definition of dP/dt, closure volume, and leakage or vortex flows. By the mid-1990s, an extended list of inception mechanisms had been proposed and included water hammer or column separation, squeeze flow through the valve gaps at the moment of closure, occluder rebound, vortex cavitation, and the venturi effect [5–8]. In addition, Wu [5] and Bluestein [6] suggested that multiple mechanisms may play simultaneous roles in cavitation inception.

The loading rate, dP/dt, where P is the transvalvular pressure gradient prior to closure, has been considered important to cavitation inception scaling since Leuer [2] discussed mechanisms of cavitation in mechanical heart valves. Use of this term arises from

the physiological definition describing the contractility, or strength of contraction during systole [9]. Graf [4], Guo [10,11], and Bluestein [12], attempted to correlate cavitation inception to the maximum value of dP/dt. However, since this maximum occurs after valve closure [13], it was quickly dropped from use. An alternate definition used by Richard [14] was the maximum dP/dt just prior to valve closure. Using this definition, it was determined that in general, as valve size increased, the threshold value of dP/dt at which cavitation inception occurred, decreased. Lee [8] found similar results with a burst tester using the average dP/dt prior to valve closure.

Carey [15] reported on an interlaboratory study to determine an FDA protocol to measure cavitation inception. Out of this study came a standard FDA definition of loading rate; "dP/dt must be averaged over the last 20 ms prior to mitral valve closure [16]." Results of this study showed great lab-to-lab variability in the value of dP/dt at cavitation inception and indicated that the most consistent results were obtained in facilities incorporating a single valve in an oscillating fluid system open to atmosphere rather than in a mock circulatory loop. More recently Chandran [17] proposed integrating the transvalvular pressure gradient over the full closure time. In practice, Rau [18] showed a very weak correlation between valve size and dP/dt in a mock loop using the FDA definition. Mixed results from a burst tester were reported by Zapanta [19], who found a similar correlation as the earlier references [8,14] for some valves but found no correlation for other valves of similar design.

In order to help isolate the drivers of cavitation in mechanical heart valves, a number of analytical models have been proposed. These models focus on prediction of the leaflet rotational velocity at closure. Cheon [20] developed a model based on a control volume approach and was able to reasonably predict the closing motion and rebound characteristics of the leaflet. More recently

---

Fig. 1 Bileaflet mechanical heart valve model

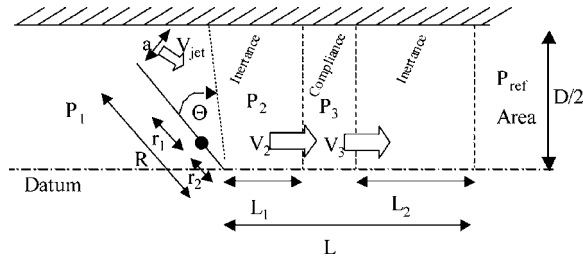
Fig. 2 Enlargement of jet region

Myers [21] proposed a simple analytical model based on an impulsive motion approximation using, as inputs, pressure wave forms, and valve geometry from Carey [15]. This model showed good agreement with experimentally determined valve closing times and rotational velocities.

While these models predict the leaflet closing dynamics, they do not couple valve motion to the resulting pressure field generated at closure and hence are unable to predict cavitation inception. Analysis of transient fluid systems is comprehensively described in Wylie [22] and Brennen [23]. Analytical models based on a lumped parameter approach or method of characteristics have been successfully applied to model closing dynamics of check valves [[24,25], among others].

This investigation continues the work reported by Maines [26] using a lumped parameter modeling approach to develop a set of differential equations, which can then be solved numerically to predict the minimum pressure within a mechanical heart valve during closure. In order to ultimately investigate the various geometric parameters and mechanisms of cavitation inception, this method incorporates both valve and facility geometry and predicts both flow rate through the valve and pressure downstream up to the point of closure. Since the lumped parameter approach allows for the addition of mechanisms such as the vortex cavitation model as described by Rambod [27] or Kini [28], the primary drivers of cavitation inception can be more readily investigated. Similarly, simulation outputs could be utilized as initial conditions to evaluate the effects of leaflet rebound on the pressure field. This paper describes the development of the basic model up to the point of closure, its calibration and validation at physiological conditions and a discussion relating the model predictions to the observed variability in the literature.

Description of Model

Figure 1 contains a sketch of half a bileaflet mechanical heart valve that swings through an angle Θ to close. The valve datum is considered to be a line of symmetry. The basic model components consist of a valve of radius (R) that pivots a distance r_2 from the datum, a jet flow through the variable gap width (a), and a volume of fluid swept downstream by the closing leaflet. Two inertial volumes, separated by a compliance volume are included to complete the dynamic description of the transient system. In actuality, both inertance and compliance are distributed along the discharge line. However, hydraulic practice has shown that a lumped parameter model consisting of two inertances on either side of a lumped compliance can be a reasonable first order model, at least for the low frequency components of the unsteadiness. Differential equations describing each model component are developed and solved simultaneously to determine the valve motion and minimum pressure, P_2, as a function of time. The upstream pressure, P_1, reference pressure, P_{ref}, and compliance pressure, P_3, are measured experimentally and are inputs to the simulation.

The equation of motion relating the rate of change of angular momentum to the torque applied to the leaflet can be written as
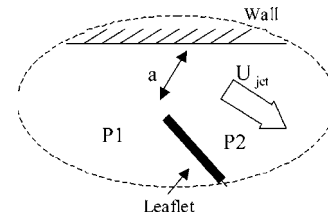
$$T = I \frac{d^2\Theta}{dt^2}. \tag{1}$$

For this model derivation, the rotational axis is assumed to be parallel to gravity, thus the torque applied to the leaflet is only a function of the pressure differential across the valve if frictional forces are neglected. Meyers [21] indicates that moments due to frictional forces in the pivot are likely small in comparison to pressure induced moments unless the leaflets are initially oriented parallel to the flow prior to closing. The torque on the leaflet is therefore simply related to the pressure difference, $P_1 - P_2$, which for simplicity will be assumed to be uniform across the leaflet and act halfway between the rotational axis and the leaflet edge on either side of the pivot, namely at r_1 and $r_2/2$. This pressure differential generates a moment $(P_1 - P_2)S_1 r_1$ where S_1 is the area outboard the axis and $r_1 = 1/2(R - r_2)$ and a moment $-(P_1 - P_2)S_2 r_2/2$ inboard of the axis.

The inertia of the leaflet is the sum of the inertia due to the leaflet mass, I_{leaf}, and an added mass of fluid accelerated by the leaflet, I_{add}. For simplification, the leaflet inertia is assumed to be that for a semi-circular plate rotating about an axis a distance r_2 from the datum while the added mass is some fraction of a cylinder of fluid swept out by the rotating leaflet. Thus the first of three calibration factors is a constant multiplying the added mass in the equation of motion.

It follows that the equation of motion becomes

$$\frac{(P_1 - P_2)}{\rho_{liquid}} = \frac{I_{leaf} + k_{add}I_{add}}{\rho_{liquid}B_1} \frac{d^2\Theta}{dt^2} \tag{2}$$

where $B_1 = S_1 r_1 - S_2 r_2/2$, and k_{add} is the added mass calibration factor. More complete definitions of the generated moment can be found in Cheon [20], Meyers [21], Ellis [24], and Arastu [25].

The second model component describes the jet flow rate through the variable width gap. Figure 2 contains an enlargement of this region. As the valve closes, the gap width, a, is reduced until a minimum nonzero value, a_{close} is reached. The nonzero value of the gap width simulates valve leakage that is known to occur. The fluid flow through the gap behaves as a jet and is represented in the model by a resistive term containing a loss coefficient Cd (the second calibration factor), and an inertive term that is a function of the rate of change of velocity in the jet as follows:

$$P_1 - P_2 = Cd\rho_{liquid}U_{jet}^2 + \rho_{liquid}\frac{d(aU_{jet})}{dt}. \tag{3}$$

The jet volumetric flow rate through the gap can be determined from the jet velocity. The area of the gap is simply the width, a, times a length measured along the major radius and equal to $1/2$ the valve circumference, ΠR. The jet flow rate is then

$$V_{jet} = a\Pi R U_{jet} \tag{4}$$

where the time dependent gap width is

$$a = a(t) = a_{close} + R(\Theta_{close} - \Theta). \tag{5}$$

Substituting for U_{jet} from Eq. (4), the jet Eq. (3) becomes

$$\frac{P_1 - P_2}{\rho_{\text{liquid}}} = Cd\left(\frac{V_{\text{jet}}}{\Pi Ra}\right)^2 + \frac{1}{\Pi R}\frac{d(V_{\text{jet}})}{dt}. \qquad (6)$$

The distributed downstream inertance and compliance of the system will be described as two lumped inertances separated by a lumped compliance. The two inertances are used to represent the inertia of the mass of fluid in the discharge line while the compliance represents the compressibility of that line. Referring back to Fig. 1, the downstream volume is represented by an inertance volume of fluid at a pressure P_2 and flow rate V_2 that enters a compliance volume at pressure P_3. A second inertance volume is placed downstream of the compliance with a flow rate V_3 that exits at a length L downstream of the valve. Three equations will be developed to describe each component beginning first with the inertance equations followed by the system compliance.

The inertance equation of the fluid immediately downstream of the valve is

$$\frac{P_2 - P_3}{\rho_{\text{liquid}}} = \frac{L_1}{A}\frac{dV_2}{dt}. \qquad (7)$$

The inertance equation for the fluid exiting at the reference plane a distance L downstream of the valve is

$$\frac{P_3 - P_{\text{ref}}}{\rho_{\text{liquid}}} = \frac{L_2}{A}\frac{dV_3}{dt}. \qquad (8)$$

The compliance, C, leads to

$$V_2 - V_3 = C\frac{dP_3}{dt}. \qquad (9)$$

The flow rate V_2 is the sum of the jet flow rate in Eq. (4) and the volume swept by the semi-circular closing leaflet namely

$$V_{\text{leaf}} = \frac{d(Vol)}{dt} = k_{\text{leaf}}\frac{2}{3}R^3\frac{d\Theta}{dt}. \qquad (10)$$

Since the leaflet does not rotate about the datum, but about r_2, a final calibration factor is used to proportionally reduce the volume swept by the leaflet for simplicity.

Finally, if the pressure differential, ΔP, across the total system is denoted by

$$\Delta P = P_1 - P_{\text{ref}} \qquad (11)$$

then after combining Eqs. (7)–(11) the downstream flow characteristics can be described by

$$\frac{P_2 - P_1}{\rho_{\text{liquid}}} = \frac{L_1 + L_2}{A}\frac{dV_{\text{jet}}}{dt} + \frac{k_{\text{leaf}}2R^3(L_1 + L_2)}{3A}\frac{d^2\Theta}{dt^2}$$
$$- \frac{CL_2}{A}\frac{d^2P_3}{dt^2} - \frac{\Delta P}{\rho_{\text{liquid}}}. \qquad (12)$$

This leaves as unknowns P_2, V_{jet}, and Θ, in Eqs. (2), (6), and (12) which when solved simultaneously yield

$$\left\{\frac{I_{\text{mass}} + k_{\text{add}}I_{\text{add}}}{\rho_{\text{liquid}}B_1} + \frac{A}{\Pi R(L_1 + L_2)}\left[\frac{k_{\text{leaf}}2R^3(L_1 + L_2)}{3A}\right.\right.$$
$$\left.\left. + \frac{I_{\text{mass}} + k_{\text{add}}I_{\text{add}}}{\rho_{\text{liquid}}B_1}\right]\right\}\frac{d^2\Theta}{dt^2}$$
$$= Cd\left\{\frac{A}{\Pi R(L_1 + L_2)[a_{\text{close}} + R(\Theta_{\text{close}} - \Theta)]}\right\}^2\left\{\int_0^t \frac{\Delta P}{\rho_{\text{liquid}}}dt\right.$$
$$- \left[\frac{k_{\text{leaf}}2R^3(L_1 + L_2)}{3A} + \frac{I_{\text{mass}} + k_{\text{add}}I_{\text{add}}}{\rho_{\text{liquid}}B_1}\right]\frac{d\Theta}{dt} + \frac{CL_2}{A}\frac{dP_3}{dt}$$
$$\left. + V_0\right\}^2 + \frac{A}{\Pi R(L_1 + L_2)}\left(\frac{\Delta P}{\rho_{\text{liquid}}} + \frac{CL_2}{A}\frac{d^2P_3}{dt^2}\right). \qquad (13)$$

Inputs to Eq. (13) are the experimentally measured quantities P_1,

P_{ref}, and P_3, the total closing angle, Θ, and the initial jet flow rate, V_0 which results from an integration of Eq. (6). The remaining input parameters are known geometric quantities describing the valve and test facilities and the three constants, k_{add}, k_{leaf}, and Cd for calibration. This set of equations was programmed using a fourth order explicit Runge–Kutta ordinary differential equation solver with a maximum time step of 5.0×10^{-5} s.

Experimental Setup

A simple experiment was performed to calibrate the simulation model under physiological, noncavitating conditions using an acrylic orifice constructed with carbon leaflets to represent a size 29 bileaflet mechanical valve. The acrylic valve model was installed in the mitral position of a horizontal mock circulatory flow loop representative of the left side of the heart (Fig. 3). The loop includes ventricle and atrial chambers with aortic and mitral valves. Compliance and resistive elements can each be adjusted to maintain physiologic conditions. Pulsatile flow was generated with a ViVitro Superpump controlled with the ViVitro VIVITEST/Acquire v3.5K software.

Simultaneous pressure measurements and high-speed video were obtained to assess valve motion and closing flow characteristics and their relationship to the pressure wave form. For input to the simulation, pressures were measured 8.3 cm upstream and 7.6 cm downstream of the valve using ViVitro PT43-604 pressure transducers with an operating range of -50–300 mm Hg and natural frequency of 800 Hz in air. The location of these transducers is shown in Fig. 3 as P_1 and P_{ref}. The minimum pressure, P_2, was obtained using a PCB 105B02 high-response pressure transducer with a resolution of 0.026 mm Hg and resonant frequency greater than 250 kHz. High response pressure data were recorded at 50 kHz. This transducer was flush mounted to the orifice wall approximately 2 mm from the leaflet at an angle 45 deg to the datum as shown in Fig. 4. In order to allow leaflet insertion, the model was split in half along a line perpendicular to the datum. This construction technique required placing the transducer 45 deg to the datum to avoid the model split line. The valve leaflets were oriented with the datum vertical to minimize the effects of gravity on closure. Throughout the text, each leaflet will be designated as proximal or distal to refer to the leaflet closest to the pressure transducer or opposite the transducer respectively.

An Olympus Industrial Encore MAC PCI 2000s high-speed video camera was used to record the valve angle as a function of time and to visualize the fluid motion during closure. Images, pressure and flow rate data were captured simultaneously using the Xcitex Inc. Midas software package. Framing rates up to 2000 per second were used to record valve dynamics during closure. In order to improve optical clarity, the loop was filled with an index matched water-glycerin solution with a density of 1.75 g/cm^3 and kinematic viscosity of 3.2 cP. The loop was illuminated with white light when recording images to obtain leaflet angle as a function of time. A 300 mW argon-ion continuous wave laser was used to illuminate silicon carbide particles seeded in the fluid when obtaining flow visualization high-speed video.

Nominal physiological test conditions were established at 2 L/min (LPM) at 70 beats/min (BPM) and at 5 LPM at both 70 and 120 BPM. The systolic ratio was set at 35% for the 70 BPM test conditions and at 50% for the 120 BPM condition. Flow rates were measured approximately 34 cm downstream of the valve as shown in Fig. 3 using a Transonic ultrasonic flow meter model T-208 and C16 flow probe filtered at 30 Hz. These flow conditions resulted in three different loading rates during valve closure. For all test conditions, the mean aortic pressure was maintained at 100 mm Hg and the fluid temperature was at 25 °C.

Experimental Results

At the end of forward flow the fluid comes to a rest and slowly reverses to initiate valve closure. The reverse flow causes the leaf-
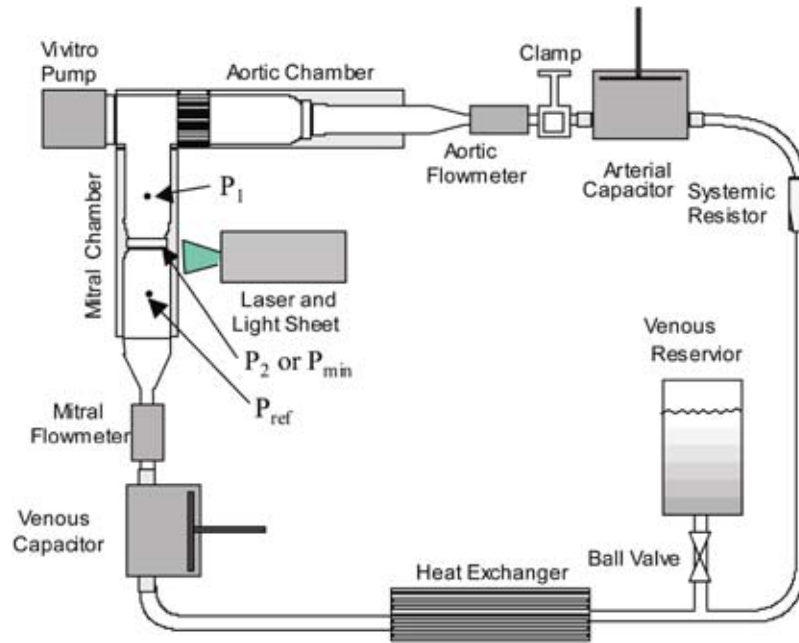
Fig. 3 Horizontal mock circulatory loop

lets to first translate with the flow prior to rotating. Once the downstream leaflet surface impacts the pivot wall and overcomes frictional resistance, rotation begins. For subsequent discussions, this instant is considered to be $t=0$. As the valve rotates to the closed position, the fluid velocity increases. Flow visualization indicates that the flow on the downstream leaflet face remains tangential to the surface and is directed toward the datum. Once the valve nears the closed position, a jet, emanating from the datum, becomes more defined and forms a vortex pair downstream of the leaflet surface similar to that observed by Manning [29]. Fluid near the leaflet tip, or outer radius, remains nearly parallel to the bulk flow direction and is observed to rapidly decelerate once the leaflets fully close. At the conditions tested, no leaflet rebounding was observed. Additionally, the vortex predicted by Avrahami [30] to form at the tip or outer radius during closure was not observed. However, a small vortex was observed to form at the perimeter after closure due to a flow reversal along the wall into the corner junction formed by the closed leaflet and wall. The formation of this structure appears similar to that observed by Kini [28].

In order to determine the simulation input wave forms and total closing angles, high-speed video was reviewed to determine the start and end of closure as well to measure the leaflet angle as a function of time. As no centerline reference was available on the model, leaflet angles were measured relative to the fully opened position. The total closure angle showed a cycle-to-cycle variation up to ±5 deg. Given the fixed closed position, this equates to different initial open angles at the start of closure. Figure 5 shows examples of pressure wave forms for three different cycles at cardiac outputs of 2 LPM identified by circles and 5 LPM by squares, each at 70 BPM. This graph shows the pressure differential (ΔP), across the valve chamber or the difference between P_1 and P_{ref} (these are simulation inputs). Leaflets were observed to close synchronously and highly asynchronous with no consistent leaflet closing order when the datum was oriented vertically. Event No. 2 at 5 LPM is an example of a synchronous closing event while event No. 6 is highly asynchronous. The measured closing time difference between leaflets was similar to those observed by Johansen [31]. Note that as the closure became more asynchronous, closing occurred longer after the sudden change in slope at a higher ΔP. It was noted after collecting data at the 5 LPM, 120 BPM test condition, that the valve had slightly rotated giving rise to asynchronous closure. It can also be observed
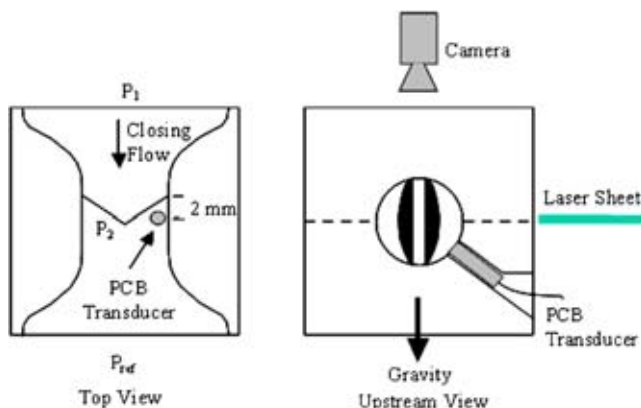

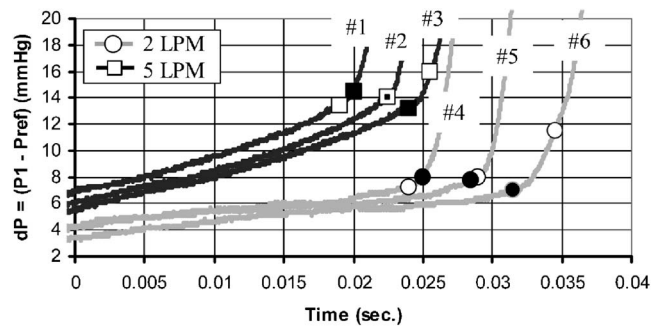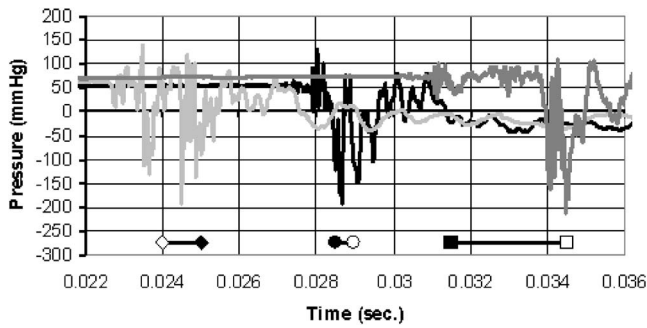**Fig. 4 Details of the acrylic valve model**

Fig. 5 Typical loading rates during valve closure. Symbols represent the closure time of each leaflet. (Open=leaflet proximal to pressure transducer; solid=distal leaflet).

Fig. 6 Typical pressure wave forms (P_2) measured ~2 mm downstream of the leaflet surface. Symbols represent the closure time of each leaflet. Open=leaflet proximal to pressure transducer; solid=distal leaflet.

that closure initiates at a finite pressure differential. This is consistent with waveforms reported by Carey [15] and used by Meyers [21] as simulation inputs.

In most cases, the minimum pressure was observed to occur immediately prior to closure of the last leaflet similar to measurements reported by Wu [32]. Figure 6 contains a plot of the high response pressure transducer placed near the valve for the same 2 LPM cycles plotted in Fig. 5. This pressure is representative of the simulation output pressure P_2. The development of the minimum pressure shows a range of behaviors. Synchronous closures similar to the event occurring around 0.028 s typically show a transient immediately prior to leaflet closure while more asynchronous closures may exhibit several distinct negative transients separated in time. Using a similar transducer placement at 45° to the rotation axis of a mono-occluder, Wu [32] measured similar dual peaks at closure. Pressure trends at this measurement position were found to track those obtained at the major radial distance although with a slight reduction in magnitude. For the closure occurring around 0.024 s, a first peak is observed prior to closing of the proximal leaflet with a second stronger peak occurring prior to distal leaflet closure. Early closure of the distal leaflet as seen for the latest event, has only minimal effect on the pressure signal with the large peaks occurring immediately prior to and at or after closure of the proximal leaflet.

Calibration of Simulation

High-speed video and pressure wave form data were analyzed for each run to determine an appropriate calibration case. Since the simulation assumes symmetry and therefore synchronous closure a single cycle at the 2 LPM, 70 BPM test condition was selected as the calibration case since the leaflets were observed to close simultaneously. Experimental pressure wave forms for P_1 and P_{ref} collected during this run were smoothed using a running average technique to minimize any discontinuities. The geometric input parameters for this run are listed in Table 1. As no measurement of the initial jet flow rate was made, it was assumed to be zero for the purposes of calibration. Similarly, since the test was conducted using a rigid acrylic model, the compliance was assumed to be zero.

The constants of calibration, k_{add}, k_{leaf}, and Cd were varied over a range of values until the predicted closing time matched the experiment. The values of k_{add}, k_{leaf}, and Cd selected using this calibration method, were 0.3, 0.25, and 0.8, respectively. Figure 7 shows the predicted pressure time history of the simulation, $P_2(t)$ as compared to the experimental time trace. While the minimum pressure is observed to occur earlier in the experiment, the simulation does predict the minimum pressure to occur prior to closure, typically within the last 0.5 deg. This prediction is consistent with two-dimensional and three-dimensional computational results for a bileaflet valve generated by Lai [33]. Using these fixed
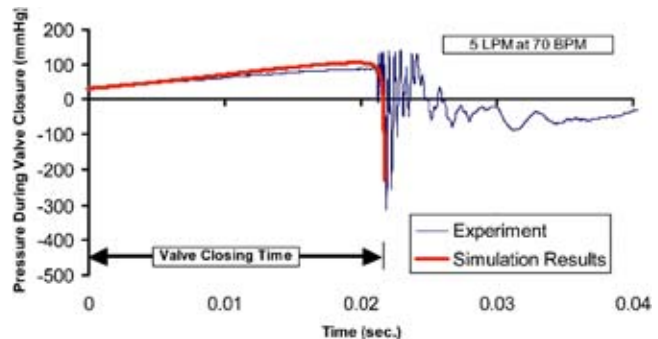
calibration values, the remaining experimental pressure traces were smoothed and used as input to the simulation along with the appropriate closing angle for each run as determined from high-speed video. Figure 8 contains a plot comparing the experimental measurement to the predicted pressure trace for a cycle at the 5 LPM, 70 BPM test condition with synchronous leaflet closure. The simulation predicts a negative pressure transient to occur at a similar time as that determined experimentally and shows reasonable agreement in magnitude.

Discussion

The closing characteristics predicted by the simulation show trends similar to the experimental data. Figure 9 contains a plot of the experimentally measured closing time versus the predicted closing time for each cycle analyzed. Included in the graph is a line representing a one-to-one correlation between the simulation and experiment. As is seen, there is good agreement for runs at the
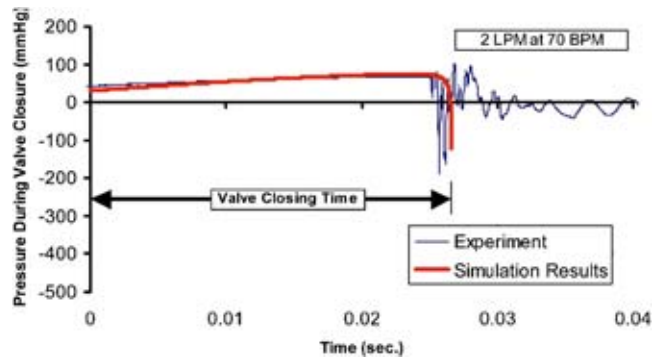
Fig. 7 Comparison of the predicted minimum pressure to experiment at a low flow condition

Fig. 8 Comparison of the predicted minimum pressure to experiment at a high flow condition

Table 1 Model calibration values

Name	Variable	Value
	Facility	
Facility radius	$D/2$	26 mm
Fluid density	ρ_{fluid}	1.75 g/cm^3
Facility length	$(L1+L2)$	$(5+71)$ mm
	Leaflets	
Leaflet radius	R	13.3 mm
Minimum gap width	a_{close}/R	0.0036
Leaflet thickness	h/R	0.067
Leaflet rotation point	r_2/R	0.20
Leaflet density	$\rho_{leaflet}$	2.0 g/cm^3
Closing angle	Θ	43.0 deg.

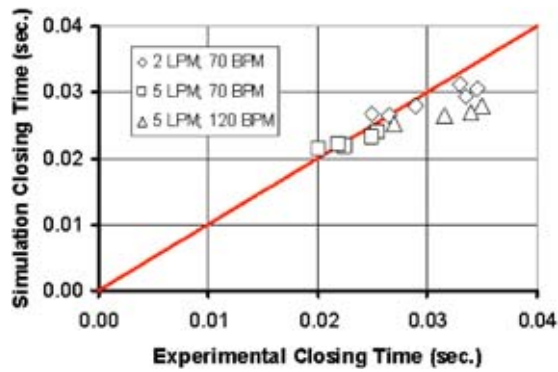**Fig. 9 Comparison of the predicted closing time to experiment**

Fig. 11 Comparison of the predicted angular position to experiment

70 BPM test condition. However, the simulation time predicted for runs at the 120 BPM condition is consistently lower than experiment. Similarly, the predicted trend for minimum pressure shows good agreement with the experiments as shown in Fig. 10 for the 70 BPM test conditions but not for the 120 BPM test runs. This deviation is likely because runs at the 120 BPM test condition exhibited asynchronous closing characteristics since the valve datum was slightly rotated from the vertical. Since the simulation assumes symmetry, it could be expected that predictions for the 120 BPM condition would show poor correlation to experiment.

Predicted leaflet angular velocities were also found to be similar to the experimental data determined from high-speed video. Figure 11 compares the predicted leaflet angle to the experimentally measured angle as a function of time for the two synchronous runs at 2 and 5 LPM. It is interesting to note that the leaflet motions for the two experimental traces remain similar prior to 0.015 s but then quickly diverge showing the leaflet reaching the closed position earlier at the 5 LPM test condition. The simulation predicts similar angular velocities near valve closure but does not predict the behavior early in the closing phase. The angular velocities at closure and loading rates for each test condition were averaged and compared to previously unpublished experimental data for a size 29 CarboMedics Inc. bileaflet mechanical valve [34], obtained in conjunction with Chandran [17]. These unpublished data were obtained using a laser sweeping technique to determine leaflet tip velocities over the last 2 deg of closure. The mean loading rate or dP/dt was calculated as proposed by Chandran [17] using

$$\frac{d(P_1 - P_{\text{ref}})}{dt} = \frac{2\int_0^{t_{\text{close}}} (P_1 - P_{\text{ref}})dt}{t_{\text{close}}^2}$$

where t_{close} is the time to reach closure. While a different test setup and fluid were used for these experiments, the trend and magnitudes predicted correlate well with Chandran [34] as seen in Fig. 12. An additional set of simulation runs was performed for a nominal closing angle of 45 deg using a constant loading rate or dP/dt rather than the experimental wave forms. These data are plotted in Fig. 12 as a solid line and show a behavior similar to that measured by Chandran [34].

As mentioned previously, the initial and final conditions were found to vary considerably from cycle-to-cycle. Thus, a set of simulations were run using a constant dP/dt to assess the effect of a nonzero initial flow rate prior to rotation as well as a change in the closure angle. Figure 13 contains a graph demonstrating that small changes in the initial or final conditions can have a significant effect on the minimum pressure. Additionally, the shape of the loading rate curve appears to play a significant role in the ultimate value of minimum pressure as demonstrated in Fig. 14, which contains a plot of loading rate versus minimum pressure comparing simulation to experimental results. Note that while the simulations using the experimental waveforms compare reasonably well to experiment at the 70 BPM test conditions, simulation runs using constant loading rates significantly over predict the minimum pressure. The solid lines in the figure demonstrate the potential variation as predicted by the simulation simply due to different initial flow rates or final closing angles. Again, results for asynchronous closure, characteristic of the 120 BPM test condition, do not appear to be well predicted by the simulation. Overall, these results suggest that a wide variation in minimum pressures is
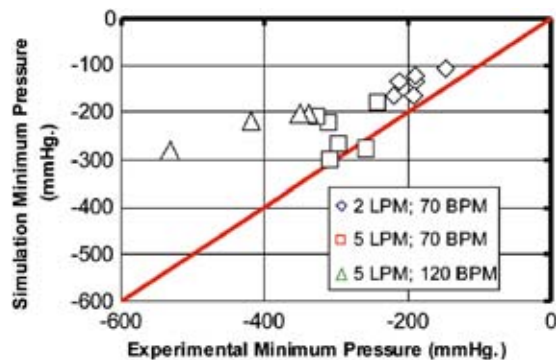

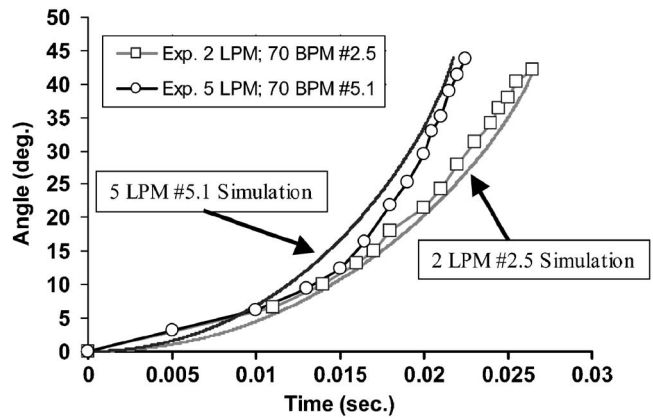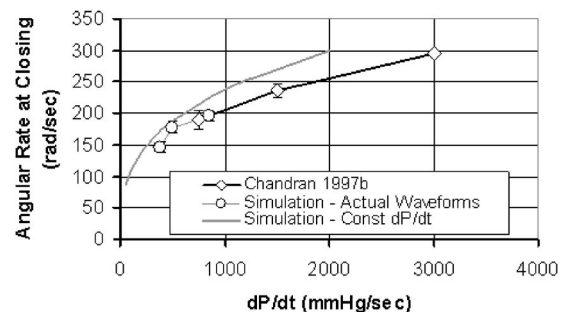**Fig. 10 Comparison of the predicted minimum pressure (P_2) to experiment**

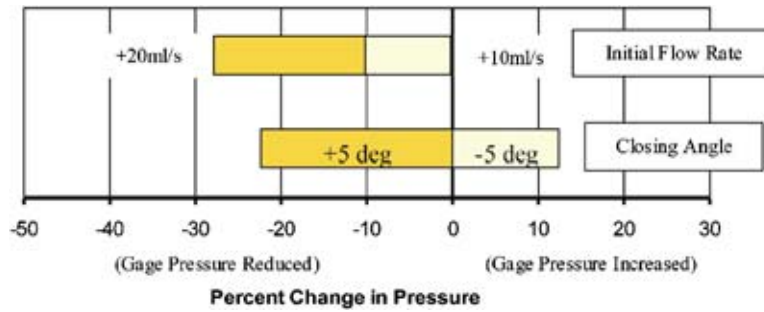**Fig. 12 Predicted angular rates at closure match experimental trends**

Fig. 13 Predicted minimum pressure is significantly affected by a change in initial or final conditions for a constant $dP/dt=200$ mm Hg/s

likely to occur experimentally for a given loading rate due to a variation in initial or final conditions, loading wave forms and the degree of asynchronous leaflet motion. This is consistent with the variability in reported loading rates measured for cavitation inception in the literature for any given valve [15,18,19].

Conclusions

A set of ordinary differential equations describing a mechanical heart valve leaflet and the fluid motion was developed to predict the minimum pressure during valve closure. In addition, experiments were conducted in a mock circulatory loop using an optically transparent size 29 bileaflet valve over a range of conditions to calibrate and validate this model at physiological conditions. Experimental results show that the minimum pressure can occur within an interval of time surrounding the instant of closure. Synchronous closing events exhibit a negative pressure transient immediately prior to closure while multiple peaks may be observed for highly asynchronous closing events; one prior to closure and one likely due to flow deceleration after closure.

Based on these experimental data, a single synchronous closing cycle was selected to calibrate the simulation model. Using this fixed calibration, a comparison to the remaining set of experimental data and other data from literature shows that the valve dynamics and negative pressure transient are well predicted by the simulation for synchronous closures. Finally, the simulation suggests that the variability observed experimentally when using dP/dt alone as the primary measure of cavitation inception is predictable.

Given the modular nature of this approach, future work should expand the simulation to address the effects of asynchronous closure and other inception mechanisms though the inclusion of additional models to more closely match the experimental results. Additional refinements should also consider the effect of gravity,

valve rebound, and the dependence on calibration factors in the equation of motion. Naturally, continued validation of this model over a range of conditions up to cavitation inception is required to determine if the effects of valve and facility geometry are appropriately modeled. Once validated, it then becomes possible to explore various mechanisms of cavitation inception and with nondimensonalization of the equations, to determine whether or not a simple scaling law can be derived. Overall, results from the current form of this lumped parameter model indicate that it is a good engineering assessment tool.

Nomenclature

Symbols

$$
\begin{aligned}
A &= \text{facility cross-sectional area} \\
a &= \text{gap width} \\
C &= \text{compliance} \\
Cd &= \text{jet loss coefficient} \\
D &= \text{facility diameter} \\
L,L_1,L_2 &= \text{lengths} \\
I &= \text{inertia} \\
h &= \text{leaflet thickness} \\
k &= \text{calibration factor} \\
P &= \text{pressure} \\
P_1 &= \text{upstream pressure} \\
P_2 &= \text{minimum pressure} \\
P_3 &= \text{compliance pressure} \\
R &= \text{valve radius} \\
r_1 &= \text{distance to pivot} \\
r_2 &= \text{pivot location} \\
S &= \text{area} \\
T &= \text{torque} \\
t &= \text{time} \\
U &= \text{velocity} \\
V &= \text{flow rate} \\
\Theta &= \text{closing angle} \\
\rho &= \text{density}
\end{aligned}
$$

Subscripts

$$
\begin{aligned}
\text{add} &= \text{added mass} \\
\text{close} &= \text{instant of valve closure} \\
\text{jet} &= \text{jet flow through gap} \\
\text{leaf} &= \text{leaflet} \\
\text{liquid} &= \text{test fluid} \\
\text{min} &= \text{minimum} \\
\text{ref} &= \text{reference} \\
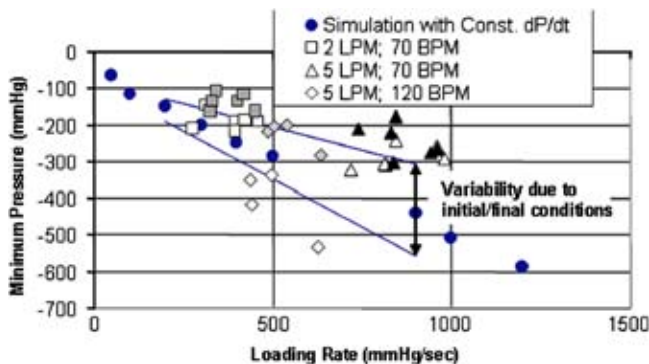0 &= \text{initial}
\end{aligned}
$$

Fig. 14 Simulation suggests that cavitation inception trends developed using the loading rate are likely to produce inconsistent results due to the variability in initial or final conditions and waveform shape. Solid=simulation; open=experimental.

References

[1] Klepetko, W., Moritz, A., Mlczoch, J., Schurawitzki, H., Domanig, E., and Wolner, E., 1989, "Leaflet Fracture in Edward-Duromedics Bileaflet Valves," J. Thorac. Cardiovasc. Surg., **97**, pp. 90–94.
[2] Leuer, J. H., 1987, "Dynamics of Mechanical Valves in the Artificial Heart,"

40th ACEMB, Niagara Falls, NY, September 10–12, p. 3.

[3] Stinebring, D. R., Lamson, T. C., and Deutsch, S., 1991, "Techniques for In Vitro Observation of Cavitation in Prosthetic Heart Valves," *ASME Cavitation and Multiphase Flow Forum*, Portland, Oregon, pp. 119–124.

[4] Graf, T., Fischer, H., Reul, H., and Rau, G., 1991, "Cavitation Potential of Mechanical Heart Valve Prostheses," Int. J. Artif. Organs, **14**, pp. 169–174.

[5] Wu, J, Wang, Y., and Hwang, N. H. C., 1994, "Occluder Closing Behavior: A Key Factor in Mechanical Heart Valve Cavitation," J. Heart Valve Dis., **3** (Suppl. I), pp. S25–S34.

[6] Bluestein, D., Einav, S., and Hwang, N. H. C, 1994, "A Squeeze Flow Phenomenon at the Closing of a Bileaflet Mechanical Heart Valve Prosthesis," J. Biomech., **27**(11), pp. 1369–1378.

[7] Makhijani, V. B., Siegel, J. M., and Hwang, N. H. C, 1996, "Numerical Study of Squeeze-Flow in Tilting Disc Mechanical Heart Valves," J. Heart Valve Dis., **5**, pp. 97–103.

[8] Lee, C. S., Chandran, K. B., and Chen, L. D., 1994, "Cavitation Dynamics of Mechanical Heart Valve Prostheses," Int. J. Artif. Organs, **18**(10), pp. 758–767.

[9] Guyton, A. C., 1981, *Textbook of Medical Physiology*, 6th ed., W. B. Saunders Company, Philadelphia.

[10] Guo, G. X., Xu, C. C., and Hwang, N. H. C., 1990, "Laser Assessment of Leaflet Closing Motion in Prosthetic Heart Valves," ASME J. Biomech. Eng., **12**, pp. 477–481.

[11] Guo, G. X., Xu, C. C., and Hwang, N. H. C., 1990, "The Closing Velocity of Baxter Duromedic Heart Valve Prostheses," ASAIO Trans., **36**, pp. M529–M532.

[12] Bluestein, D., Menon, S., Wu, Z., Haubold, A., Armitage, T., and Hwang, N., 1993, "Closing Behavior of a New Bileaflet Mechanical Heart Valve," ASAIO J., **39**, pp. M398–M402.

[13] Wu, J., and Hwang, N. H. C., 1995, "Ventricular Pressure Slope and Bileaflet Mechanical Heart Valve Closure," ASAIO J., **41**, pp. M763–M767.

[14] Richard, G., 1992, "Cavitation in Bi-Leaflet Valves," Carbomedics Report, TR–0086–1.

[15] Carey, R. F., Porter, J. M., Richard, G., Luck, C., Shu, M. C. S., Gou, G. X., Elizondo, D. R., Kingsbury, C., Anderson, S., and Herman, B. A., 1995, "An Interlaboratory Comparison of the FDA Protocol for the Evaluation of Cavitation Potential of Mechanical Heart Valves," J. Heart Valve Dis., **4**, pp. 532–541.

[16] *Replacement Heart Valve Guidance; Draft Document*, 1994, U.S. Department of Health and Human Services, Office of Device Evaluation, October.

[17] Chandran, K. B., and Aluri, S., 1997, "Mechanical Valve Closing Dynamics: Relationship Between Velocity of Closing, Pressure Transients and Cavitation Initiation," Ann. Biomed. Eng., **25**, pp. 926–938.

[18] Rau, G., and Reul, H., 1998, "In Vitro Cavitation Analysis of Sulzer Carbomedics Bileaflet Mechanic Heart Valve Prostheses According to FDA-Draft Replacement Heart Valve Guidance, Version 4.1 Appendix H," Carbomedics Internal Report.

[19] Zapanta, C. M., 1999, "Determination of Appropriate Test Variables to Evaluate the Cavitation Potential of Prosthetic Heart Valves," Carbomedics Draft Report TR–1912.

[20] Cheon, G., and Chandran, K. B., 1994, "Transient Behavior Analysis of a Mechanical Monoleaflet Heart Valve Prosthesis in the Closing Phase," ASME J. Biomech. Eng., **116**, pp. 452–458.

[21] Meyers, M. R., and Porter, J. M., 2003, "Impulsive Motion Model for Computing the Closing Motion of Mechanical Heart Valve Leaflets," Ann. Biomed. Eng., **31**, pp. 1031–1039.

[22] Wylie, E. B., and Streeter, V. L., 1993, *Fluid Transients in Systems*, Prentice Hall, Upper Saddle River, NJ.

[23] Brennen, C. E., 1994, *Hydrodynamics of Pumps*, Concepts ETI, Norwich Vermont and Oxford University Press, New York.

[24] Ellis, J., and Mualla, W., 1986, "Numerical Modeling of Reflux Valve Closure," ASME J. Pressure Vessel Technol., **108**, pp. 92–97.

[25] Arastu, A. H., and Husaini, S. M., 1995, "A Comprehensive Check Valve Dynamics Model for Water," *Proc. ASEM Fluids Eng. Div.*, FED-Vol 234, IMECE.

[26] Maines, B. H., and Brennen, C. E., 2001, "Applicability of Fluid Transient Test Methods for Mechanical Heart Valve Cavitation Scaling," *Sixth Annual Hilton Head Workshop sponsored by the Parker Institute for Bioengineering and Bioscience. Prosthetic Heart Valves: Past Present and Future*.

[27] Rambod, E., Beizaie, M., Shusser, M., Milo, S., and Gharib, M., 1999, "A Physical Model Describing the Mechanism for Formation of Gas Microbubbles in Patients with Mitral Mechanical Heart Valves," Ann. Biomed. Eng., **27**, pp. 774–792.

[28] Kini, V., Bachmann, C., Fontaine, A., Deutsch, S., and Tarbell, J. M., 2000, "Flow Visualization in Mechanical Heart Valves: Occluder Rebound and Cavitation Potential," Ann. Biomed. Eng., **28**(4), pp. 431–441.

[29] Manning, K. B., Kini, V., Fontaine, A. A., Deutsch, S., and Tarbell, J. M., 2003, "Regurgitant Flow Field Characteristics of the St. Jude Bileaflet Mechanical Heart Valve under Physiologic Pulsatile Flow using Particle Image Velocimetry," Artif. Organs, **27**(9), pp. 840–846.

[30] Avrahami, I., Rosenfeld, M., Einav, S., Eichler, M., and Reul, H., 2000, "Can Vortices in the Flow Across Mechanical Heart Valves Contribute to Cavitation?" Med. Biol. Eng. Comput., **38**, pp. 93–97.

[31] Johansen, P., Manning, K. B., Tarbell, J. M., Fontaine, A. A., Deutsch, S., and Nygaard, H., 2003, "A New Method for Evaluation of Cavitation Near Mechanical Heart Valves," ASME J. Biomech. Eng., **125**, pp. 663–670.

[32] Wu, J., Gao, B. Z., and Hwang, N. H. C., 1995, "Transient Pressure at Closing of a Monoleaflet Mechanical Heart Valve Prosthesis: Mounting Compliance Effect," J. Heart Valve Dis., **4**, pp. 553–567.

[33] Lai, G. Y., and Chandran, K. B., 2001, "Simulation of Mechanical Heart Valve Closure Dynamics: Present Status and Future Directions," *Sixth Annual Hilton Head Workshop sponsored by the Parker Institute for Bioengineering and Bioscience. Prosthetic Heart Valves: Past Present and Future*.

[34] Chandran, K. B., 1997, "Measurement of Velocity of the Occluder at Valve Closure," Carbomedics Inc. Internal Report.